

Cancrinite: Crystal structure, phase transitions, and dehydration behavior with temperature

ISHMAEL HASSAN,^{1,*} SYTLE M. ANTAO,² AND JOHN B. PARISE²

¹Department of Chemistry, University of the West Indies, Mona, Kingston 7, Jamaica

²Mineral Physics Institute and Department of Geosciences, State University of New York, Stony Brook, New York 11794-2100, U.S.A.

ABSTRACT

The structural behavior of a cancrinite, $\text{Na}_{5.96}\text{Ca}_{1.52}[\text{Al}_6\text{Si}_6\text{O}_{24}](\text{CO}_3)_{1.57} \cdot 1.75\text{H}_2\text{O}$, was determined by using in situ synchrotron X-ray powder diffraction data [$\lambda = 0.91806(5) \text{ \AA}$] at room pressure and from 25 to 982 °C. The sample was heated at a rate of about 9.5 °C/min, and X-ray traces were collected at about 15 °C intervals. The satellite reflections in cancrinite were lost at about 504 °C, where a phase transition occurs. All the unit-cell parameters for cancrinite also show a discontinuity at 504 °C. Initially, the $[\text{Ca}\text{-CO}_3]$ clusters and their vacancies are ordered in the channels, and this ordering is destroyed on heating to give rise to the phase transition. Cancrinite loses water continuously until about 625 °C; thereafter an anhydrous cancrinite phase exists. From 25 to 952 °C, a minimal amount of CO_2 is lost from the structure. Over this temperature range, the average $\langle\text{Al-O-Si}\rangle$ bridging angle, which is an indication of the degree of rotation of the tetrahedra, increases from 143.7(4) to 147.7(5)°. Rotations of the tetrahedra are caused by expansion of the Na1-O2 bond lengths.

Keywords: Cancrinite, high-temperature structure, phase transitions, dehydration, Rietveld refinements, synchrotron radiation

INTRODUCTION

The cancrinite-group minerals are of interest because they are framework rock-forming aluminosilicate minerals that contain volatile elements, and share structural units with the industrially important zeolites. The cages in cancrinite (ϵ -cage) are the same as the building units in many zeolites. The cancrinite-group minerals have complicated and rather interesting chemistries; they contain large anionic groups, and many are nonstoichiometric. Structurally, they are of special interest because they display intriguing satellite reflections that vary markedly with composition and temperature, thus giving rise to complicated modulated structures.

The structure of cancrinite consists of a network of TO_4 (T = Al, Si) tetrahedra in which the T atoms are fully ordered (Fig. 1). The structure contains parallel six-membered rings consisting of alternating AlO_4 and SiO_4 tetrahedra. These rings are stacked in an *ABAB...* sequence and give rise to $P6_3$ hexagonal symmetry and large continuous channels parallel to the 6_3 axes (= z axis); the channels are bounded by twelve-membered rings of alternating AlO_4 and SiO_4 tetrahedra. The cancrinite structure also consists of “columns” of small ϵ -cages that are bounded by six four-membered and five six-membered rings consisting of alternating AlO_4 and SiO_4 tetrahedra. These cages occur along the threefold axes that are parallel to the z axis.

The structures of several cancrinite specimens are known (e.g., Nithollon and Verotte 1955; Jarchow 1965; Smolin et al. 1981; Emiraliev and Yamzin 1982; Grundy and Hassan 1982; Kanepit and Nozik 1985; Ballirano and Maras 2004). The ϵ -cages in cancrinite, vishnevite, pitiglianoite, and hydroxycancrinite contain a $[\text{Na}\cdot\text{H}_2\text{O}]^+$ cluster, whereas in davyne, quadridavyne,

and microsommite the cage contains a Ca and a Cl atom, while tiptopite contains a K atom in a cage (e.g., Hassan and Grundy 1990; Bonaccorsi et al. 1990, 1994, 2001; Merlino et al. 1991; Peacor et al. 1987). In cancrinite, the Na atoms are on the Na1 site in the ϵ -cages, and the oxygen of the H_2O molecule, denoted O_w , is disordered around the threefold axis to form favorable hydrogen bonds and reasonable Na- O_w distances (Fig. 1). In davyne, for example, Ca rather than Na atoms occur on the Na1 site, and Cl atoms occur on the threefold axis in place of the disordered O_w . The channels contain the remaining cations (Na^+ , Ca^{2+} , and K^+ on the Na2 site) and anions (CO_3^{2-} , SO_4^{2-} , OH^- , and H_2O ; e.g., Hassan and Grundy 1984, 1990, 1991). Vacancies are present in the channels.

In the average substructure of cancrinite, the C atoms of the CO_3 group are at (0, 0, z), and occupy two split positions: C1 and C2 (and their symmetry related positions C1' and C2'). All four C positions are statistically equally occupied with a site occupancy factor (*sof*) of 0.38 (Grundy and Hassan 1982). This suggests the possibility of ordering of the CO_3 groups and vacancies, and the formation of superstructures. The ordering is associated with subsequent re-arrangement of the cations and vacancies on the Na2 site.

Satellite reflections are commonly observed in cancrinite-group minerals, but their origins are not known in detail (Jarchow 1965; Foit et al. 1973; Brown and Cesbron 1973). The satellite reflections indicate distinct supercells with various values for the c parameter. Details of the satellite reflections from cancrinite-group minerals differ for each mineral and differ in specimens from different localities. The structural model of Grundy and Hassan (1982) was confirmed by Hassan and Buseck (1992) using high-resolution transmission electron microscopy (HRTEM). In addition to distinct chemistries, the satellite reflections are related to ordering of the ions in the channels. The CO_3 -group

* E-mail: ishmael.hassan@uwimona.edu.jm

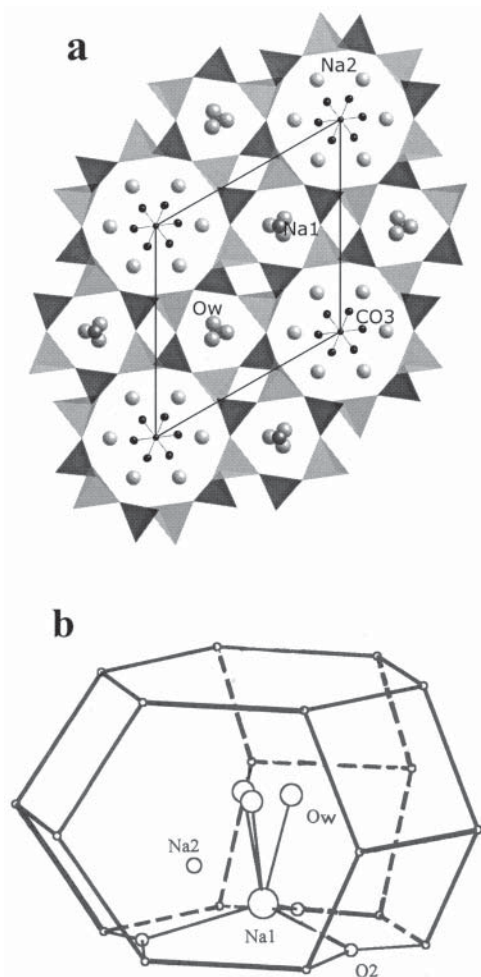


FIGURE 1. Crystal structure of cancrinite showing the location of the atoms in the cages and channels. The Al and Si tetrahedra are ordered. (a) Projection of the structure along [001] (after Grundy and Hassan 1982), and (b) a cancrinite cage showing the location of Na1 and Na2 sites, and the disordered O_w water molecules.

vacancies are associated with Ca-atom vacancies, and these $[Ca-CO_3]$ vacancies are ordered in the channels and give rise to the supercell in cancrinite. The superstructure in cancrinite should be destroyed on heating, resulting in a phase transition and a true cancrinite subcell. Although previous high-temperature structural studies are not available for natural cancrinites, a recent study was done on a synthetic cancrinite (Weller and Kenyon 2004). There are several aims to this study: (1) determine accurate unit-cell parameters with temperature to detect the expected phase transitions; (2) observe the temperature where the satellite reflections are lost and the phase transition occurs; (3) follow the structural changes across the phase transition using in situ diffraction data and Rietveld refinements; (4) follow the loss of structural water and compare it with a previous DTA study (Hassan 1996a); and (5) determine the crystal structure of the anhydrous cancrinite phase.

EXPERIMENTAL METHODS

The pinkish white cancrinite sample used in this study is from Dungannon Township, Bancroft, Ontario, and is well characterized (e.g., Grundy and Hassan

1982; Hassan and Buseck 1992). The chemical composition is $Na_{5.96}Ca_{1.52}[Al_6Si_6O_{24}](CO_3)_{1.57} \cdot 1.75H_2O$ with $P6_3$ hexagonal pseudo-symmetry, cell parameters $a = 12.590(3)$, $c = 5.117(1)$ Å, and a supercell of $8 \times c$ ($= 40.94$ Å). The crystals of cancrinite were handpicked and crushed to a powder using an agate mortar and pestle. High-temperature synchrotron X-ray powder diffraction experiments were performed at beam-line X7B of the National Synchrotron Light Source at Brookhaven National Laboratory. The sample was loaded in a quartz capillary (diameter = 0.5 mm, open to air at one end) and was oscillated during the experiment over a θ range of 10° . The high-temperature X-ray data were collected using in-situ synchrotron radiation [$\lambda = 0.91806(5)$ Å] at room pressure and from 25 to 982 °C. Elevated temperatures were obtained using a horseshoe-shaped heater and controlled using a thermocouple element near the capillary. The temperature was calibrated using the 811 and 982 °C phase-transition temperatures in synthetic $BaCO_3$. Data were collected at a heating rate of about 9.5 °C/min. The data were collected in regular intervals of about 15 °C to a maximum 2θ of about 50° [$(\sin\theta/\lambda) < 0.46$ Å $^{-1}$]. An imaging plate (IP) detector (Mar345, 2300 × 2300 pixels) mounted perpendicular to the beam path was used to collect full-circle Debye-Scherrer rings with an exposure time of 10 s. An external LaB_6 standard was used to determine the sample-to-detector distance, wavelength, and tilt of the IP. The diffraction patterns recorded by the IP were integrated using the Fit2d program to produce conventional I- 2θ traces (Hammersley 1996).

Rietveld structure refinements

Several X-ray traces at regular temperature intervals were selected for treatment with the Rietveld method that is incorporated in *GSAS* and *EXPGUI* programs (Larson and Von Dreele 2000; Toby 2001). For the room temperature structure, the starting atomic coordinates, cell parameters, isotropic displacement parameters, and space group $P6_3$ were those of Grundy and Hassan (1982). The refined atomic coordinates were then used as input for the next higher-temperature structure. The site occupancy factors (*sofs*) in the structural model were initially set to the nominal chemical composition of $Na_6Ca_{1.52}[Al_6Si_6O_{24}](CO_3)_{1.52} \cdot 2H_2O$, as was done by Grundy and Hassan (1982). Subsequently, the *sofs* for the O_w site and those for the CO_3 group were refined.

The background was modeled using a twenty-four-coefficient Chebyshev polynomial function of the first kind, which models quite well the background “hump” of the quartz capillary that was used to hold the sample. The reflection-peak profiles were fitted using the pseudo-Voigt function with three refinable coefficients (GW, GV, and LY). The zero-shift was set to zero at all temperatures, as the instrument was calibrated with a LaB_6 standard. A full-matrix least-squares refinement varying a scale factor, cell parameters, atomic coordinates, and isotropic displacement parameters converged rapidly. Isotropic displacement parameters were used during the refinements, but similar atoms were constrained to have equal displacement parameters, for example, the Al and Si atoms were constrained to have equal displacement parameters, as were the atoms in the carbonate groups. Because of the complexity of the cancrinite structure, soft constraints were initially used for T-O and C-O distances [Si-O = 1.615(20), Al-O = 1.733(20), and C-O = 1.30(2) Å], and the statistical weights were subsequently decreased during the refinements until they were finally removed completely before the final cycles of refinement. Soft constraints were also used to refine the structures of other cancrinites (Burton et al. 1999; Fechtelkord et al. 2001). Finally, the background (24 terms), profile parameters (3 terms), a scale factor, cell and structural parameters (36 or 35 terms), were allowed to vary, and the refinement proceeded to convergence. At the end of the refinements, the total number of variables was either 64 or 63, and the number of observed reflections was between 232 and 240, and the number of observations (data points) was about 2000. The structures refined well at all temperatures up to 952 °C. At 982 °C, the number of observed reflection increased to 258, indicating the start of formation of an additional nepheline-like phase. Refinement of the cancrinite structure was noticeably poorer at this temperature. Representative examples of synchrotron powder X-ray diffraction (XRD) patterns are shown in Figure 2. The cell parameters and the Rietveld structure refinement statistics at various temperatures are listed in Table 1. The atom coordinates and isotropic displacement parameters are given in Table 2, and selected bond distances and angles are listed in Table 3.

RESULTS AND DISCUSSION

Satellite reflections in cancrinite

Well-developed satellite reflections occur in the sample used in this study. Such reflections are easily observed in selected-area electron diffraction (SAED) patterns (see Fig. 2 of Hassan and

TABLE 1. Unit-cell parameters for cancrinite at various temperatures (°C) and agreement factors

T/°C	a/Å	c/Å	c/a	V/Å ³	*R _f ²
SC20†	12.590(3)	5.117(1)	0.4064	702.4(3)	
25	12.5906(2)	5.1168(1)	0.4064	702.45(2)	0.0615
101	12.5979(2)	5.1243(1)	0.4068	704.30(2)	0.0586
207	12.6111(2)	5.1369(1)	0.4073	707.51(3)	0.0602
298	12.6268(2)	5.1514(1)	0.4080	711.29(3)	0.0565
344	12.6342(2)	5.1580(1)	0.4083	713.04(3)	0.0592
405	12.6414(2)	5.1641(1)	0.4085	714.69(2)	0.0612
466	12.6524(2)	5.1730(1)	0.4089	717.16(3)	0.0585
496	12.6538(2)	5.1736(1)	0.4089	717.41(3)	0.0577
511	12.6508(2)	5.1707(1)	0.4087	716.67(3)	0.0627
526	12.6571(2)	5.1755(1)	0.4089	718.05(3)	0.0578
541	12.6554(2)	5.1732(1)	0.4088	717.54(3)	0.0554
557	12.6560(2)	5.1728(2)	0.4087	717.54(3)	0.0550
602	12.6613(2)	5.1753(2)	0.4087	718.49(3)	0.0774
648	12.6696(2)	5.1801(2)	0.4089	720.10(3)	0.0789
693	12.6758(2)	5.1835(2)	0.4089	721.28(3)	0.0595
800	12.6886(2)	5.1924(2)	0.4092	723.99(3)	0.0629
891	12.7034(3)	5.2031(2)	0.4096	727.16(3)	0.0585
906	12.7053(3)	5.2043(2)	0.4096	727.55(3)	0.0638
952	12.7187(4)	5.2150(2)	0.4100	730.58(4)	0.0593
982	12.7281(5)	5.2242(3)	0.4104	732.96(6)	0.0682

* R_f² = R-structure factor based on observed and calculated structure amplitudes = $(\sum(F_o^2 - F_c^2)^2 / \sum(F_o^2)^2)^{1/2}$.

† SC20 refers to single-crystal data from Grundy and Hassan (1982) in all tables.

Buseck 1992). In X-ray precession photographs, strong satellite reflections were only observed at relatively high angles (see Fig. 2 of Grundy and Hassan 1982). In the powder synchrotron XRD traces, while several weak satellite reflections are observable at low angles, a fairly strong satellite reflection occurs at about 19° 2θ (Fig. 2a). The satellite reflections are easily seen in the difference profile trace and they were not excluded in the refinements because they are quite weak. The satellite reflections were not observed in the trace at 511 °C and indicates a phase transition (Fig. 2b).

In SAED patterns and X-ray photographs, the observed cancrinite supercell is $a \times 8c$ (i.e., 12.590 by 40.936 Å; Grundy and Hassan 1982). This supercell was refined with the room temperature data using the Le Bail method in GSAS with the background and profile terms determined by the Rietveld method for the substructure cell at 25 °C. Keeping the Rietveld terms fixed and refining only the scale and cell parameters, the supercell parameters obtained were $a = 12.5935(2)$, $c = 40.9451(7)$ Å, and $V = 5623.8(1)$ Å³ (with $R_p = 0.0138$ and $R_{wp} = 0.0190$). The strong superstructure reflection at about 19° 2θ was indexed as 1,1,13 in the supercell, and is quite close to the position where the superstructure reflections were observed in X-ray precession photographs (see Fig. 2 of Grundy and Hassan 1982). The weaker satellite reflection at about 9° 2θ was indexed as 016.

The ordering that gives rise to the satellite reflections in cancrinite is destroyed by about 504 °C (chosen between 496 and 511 °C; see Fig. 2b). The disappearance of the satellite reflections marks the onset of a structural phase transition, which results in a true cancrinite subcell. However, in a DTA-TG study, this subtle structural phase transition was not observed because of the lower sensitivity of the technique (see Hassan 1996a).

Cell parameters

The unit-cell parameters for cancrinite at 25 °C obtained in this study [Table 1; $a = 12.5906(2)$, $c = 5.1168(1)$ Å] are similar

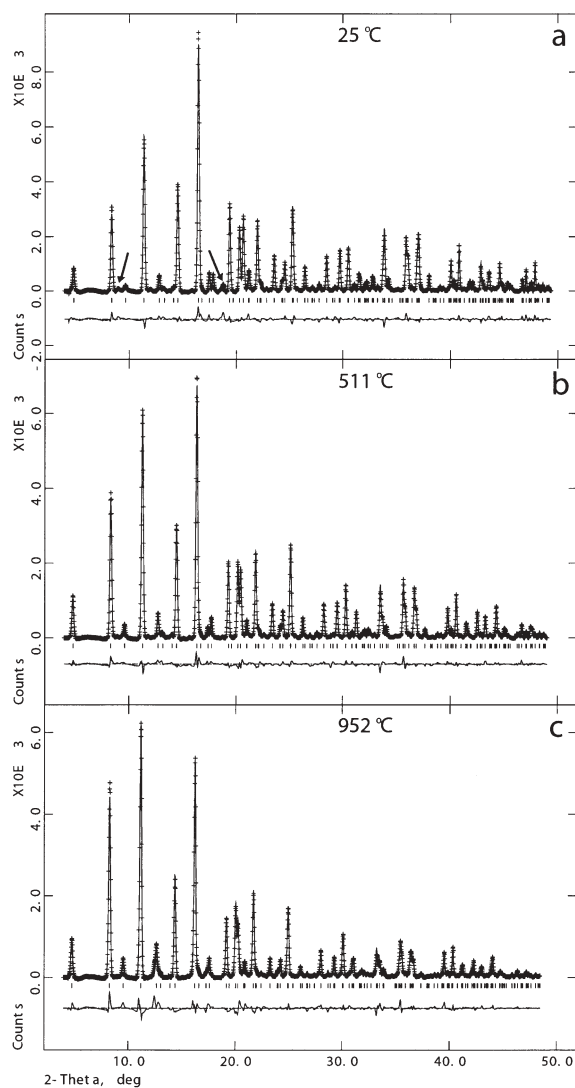


FIGURE 2. Synchrotron X-ray powder diffraction pattern for cancrinite at (a) 25 °C, (b) 511 °C, and (c) 952 °C together with the calculated and difference plot from Rietveld refinement. Satellite reflections are indicated by arrows in (a). These reflections disappear in the trace at 511 °C. New additional, very weak reflections (not seen at this scale) were observed in the trace in (c). Due to their weak intensities, the satellite reflections in a, and the additional reflections observed at 952 °C were not excluded from the refinements. For the pattern at 25 °C, the 100% peak at 16.445° 2θ is indexed as 121 or 211, and has a FWHM of 0.1867(7)°.

to those obtained by Hassan and Grundy (1982; $a = 12.590(3)$, $c = 5.117(1)$ Å). The variation of the unit-cell parameters for cancrinite with temperature is shown in Figure 3, together with solid lines or curves showing the least-squares fit to the data. All the cell parameters increase linearly to 504 °C. However, at 504 °C there is a sharp discontinuity, indicating the occurrence of a structural phase transition in cancrinite. This break in slope was not detected from the unit-cell parameters obtained from conventional powder XRD data because (1) a small number of

TABLE 2. Positional and isotropic displacement parameters ($U \times 100 \text{ \AA}^2$) at various temperatures ($^{\circ}\text{C}$) for cancrinite

Atom/T	SC20	25	101	207	298	405	496	511	557	602	
Si	x	0.3277(1)	0.3246(5)	0.3248(6)	0.3248(6)	0.3253(7)	0.3254(6)	0.3387(7)	0.3385(7)	0.3270(8)	0.3270(8)
	y	0.4104(1)	0.4029(5)	0.4024(5)	0.4022(5)	0.4021(6)	0.4037(7)	0.4165(6)	0.4162(7)	0.4092(9)	0.4097(9)
	U	0.73(3)	0.31(8)	0.34(8)	0.42(8)	0.42(8)	0.51(7)	0.82(7)	0.87(7)	1.15(7)	1.26(7)
Al	x	0.0752(1)	0.0775(6)	0.0776(6)	0.0769(6)	0.0769(7)	0.0756(7)	0.0755(7)	0.0758(7)	0.0724(8)	0.0724(8)
	y	0.4125(1)	0.4205(6)	0.4204(6)	0.4200(6)	0.4196(7)	0.4172(7)	0.4041(6)	0.4045(7)	0.4123(8)	0.4123(8)
	z	0.7510(3)	0.7612(25)	0.7618(26)	0.7622(27)	0.7599(35)	0.754(6)	0.7511(32)	0.7525(31)	0.7497(29)	0.7512(28)
O1	x	0.2027(2)	0.2051(14)	0.2057(14)	0.2070(15)	0.2068(16)	0.2049(17)	0.2114(17)	0.2113(17)	0.2015(20)	0.2020(19)
	y	0.4043(2)	0.4032(6)	0.4039(6)	0.4049(6)	0.4062(6)	0.4079(6)	0.4084(6)	0.4088(6)	0.4079(6)	0.4097(6)
	z	0.6574(5)	0.6777(21)	0.6791(21)	0.6804(23)	0.6791(26)	0.676(4)	0.6774(24)	0.6770(24)	0.6726(24)	0.6698(24)
	U	1.63(9)	1.05(13)	1.26(14)	1.59(15)	1.98(14)	2.25(13)	2.34(12)	2.25(12)	2.34(13)	2.29(13)
O2	x	0.1131(2)	0.1085(5)	0.1081(5)	0.1073(5)	0.1068(5)	0.1073(5)	0.1052(5)	0.1055(5)	0.1055(5)	0.1065(6)
	y	0.5635(2)	0.5568(14)	0.5566(14)	0.5568(15)	0.5579(15)	0.5602(14)	0.5578(20)	0.5585(19)	0.5584(17)	0.5593(17)
	z	0.7281(7)	0.7355(23)	0.7362(24)	0.7377(27)	0.7389(30)	0.748(4)	0.7412(31)	0.7423(32)	0.7439(31)	0.7461(31)
O3	x	0.0295(2)	0.0209(11)	0.0201(11)	0.0189(13)	0.0173(13)	0.0156(16)	0.0128(15)	0.0122(15)	0.0117(13)	0.0116(13)
	y	0.3487(2)	0.3515(13)	0.3503(14)	0.3483(16)	0.3442(18)	0.3407(21)	0.3360(13)	0.3352(13)	0.3373(14)	0.3371(14)
	z	0.0610(5)	0.0521(42)	0.0509(43)	0.0499(47)	0.0517(43)	0.058(4)	0.0259(32)	0.0259(32)	0.0234(30)	0.0215(31)
O4	x	0.3131(2)	0.3056(11)	0.3073(12)	0.3085(15)	0.3118(18)	0.3171(21)	0.3213(16)	0.3218(15)	0.3171(16)	0.3178(16)
	y	0.3566(2)	0.3533(12)	0.3540(13)	0.3547(15)	0.3556(17)	0.3557(19)	0.3596(12)	0.3606(12)	0.3583(14)	0.3590(13)
	z	0.0439(5)	0.0660(31)	0.0659(32)	0.0642(35)	0.0553(35)	0.041(4)	0.0642(22)	0.0662(21)	0.0661(25)	0.0677(24)
Na1	x	0.1339(11)	0.1206(21)	0.1237(22)	0.1288(24)	0.1277(26)	0.1167(35)	0.1126(24)	0.1124(24)	0.1075(26)	0.1050(27)
	U	4.91(18)	3.14(13)	3.49(14)	3.96(16)	4.42(18)	4.69(16)	5.70(18)	5.67(18)	6.60(19)	7.38(22)
Na2	x	0.1232(1)	0.1268(9)	0.1259(10)	0.1247(11)	0.1233(11)	0.1237(11)	0.1302(11)	0.1302(11)	0.1270(16)	0.1277(16)
	y	0.2490(1)	0.2509(4)	0.2508(4)	0.2508(4)	0.2505(4)	0.2522(4)	0.2512(4)	0.2514(4)	0.2523(4)	0.2530(4)
	z	0.2959(3)	0.2996(14)	0.3004(15)	0.3008(16)	0.3010(18)	0.2993(28)	0.2982(18)	0.2981(17)	0.2965(16)	0.2940(17)
	U	0.6729(25)	0.714(5)	0.720(5)	0.725(6)	0.718(7)	0.696(7)	0.691(6)	0.691(6)	0.583(8)	0.590(9)
C1	x	4.45(94)	1.8(7)	1.6(7)	2.6(8)	2.8(8)	2.8(8)	3.6(8)	3.4(8)	6.0(10)	7.4(12)
C2	z	0.9134(30)	0.940(5)	0.942(5)	0.939(7)	0.930(7)	0.913(8)	0.913(8)	0.914(8)	0.825(8)	0.835(9)
O _{C1}	x	0.0572(8)	0.0766(31)	0.0764(31)	0.0756(37)	0.0746(43)	0.0723(48)	0.0374(44)	0.0369(43)	0.0879(34)	0.0901(38)
	y	0.1163(8)	0.1131(21)	0.1127(21)	0.1125(25)	0.1135(28)	0.1147(26)	0.1154(24)	0.1153(24)	0.1112(37)	0.1096(42)
O _{C2}	x	0.0587(8)	0.0758(37)	0.0785(34)	0.0827(37)	0.0901(32)	0.0953(25)	0.0253(31)	0.0242(31)	0.0510(51)	0.0464(47)
	y	0.1194(8)	0.1197(20)	0.1203(21)	0.1222(25)	0.1221(29)	0.1136(27)	0.1225(28)	0.1237(28)	0.1237(28)	0.1263(32)
C	sof	0.380	0.380	0.380	0.380	0.380	0.380	0.380	0.380	0.380	0.380
O _w	z	0.6875(25)	0.6926(37)	0.6975(42)	0.7059(52)	0.7131(66)	0.768(10)	0.7983(99)	0.807(11)	0.798(23)	0.803(25)
O _w	sof	1.0	0.801(13)	0.788(13)	0.782(14)	0.719(14)	0.496(13)	0.288(14)	0.254(14)	0.139(14)	0.030(15)

Notes: Na1 at (2/3, 1/3, z); C1 and C2 at (0, 0, z). Constraints: z(C1) = z(O_{C1}); z(C2) = z(O_{C2}); O_w = [2/3, 1/3, z]; U(O_w) = 0.025; U(Si) = Al; U(O1) = O2 = O3 = O4; U(C1) = C2 = O_{C1} = O_{C2}; U(Na1) = U(Na2). For sof: Na1 = 1.0; Na2 = 1.125 (± 0.67Na + 0.25Ca); C1 = C2 = O_{C1} = O_{C2} = 0.38 from 25 to 602 $^{\circ}\text{C}$ and variable thereafter. For SC20, O_w is at [0.6246(12), 0.3243(42), 0.6875(25)]. Si: z = 3/4.

TABLE 3. Bond distances (\AA) and angles ($^{\circ}$) at various temperatures ($^{\circ}\text{C}$) for cancrinite

Atom/T	SC20	25	101	207	298	405	496	511	577	602
Si-O1	1.608(3)	1.552(19)	1.553(19)	1.545(19)	1.566(20)	1.597(23)	1.606(21)	1.609(21)	1.629(24)	1.636(24)
-O2	1.601(4)	1.717(16)	1.721(17)	1.714(17)	1.697(18)	1.660(16)	1.514(23)	1.511(23)	1.619(21)	1.612(22)
-O3	1.619(5)	1.508(18)	1.505(19)	1.503(21)	1.493(19)	1.482(16)	1.643(16)	1.639(16)	1.627(15)	1.640(14)
-O4	1.621(3)	1.706(17)	1.705(17)	1.698(19)	1.658(18)	1.606(18)	1.747(13)	1.750(12)	1.739(14)	1.748(13)
<Si-O>	1.612(2)	1.621(9)	1.621(9)	1.615(10)	1.604(9)	1.586(9)	1.628(9)	1.627(9)	1.654(9)	1.659(9)
Al-O1	1.728(3)	1.777(18)	1.779(18)	1.793(18)	1.781(19)	1.743(22)	1.736(22)	1.733(22)	1.710(25)	1.711(25)
-O2	1.717(3)	1.564(16)	1.565(17)	1.574(18)	1.595(18)	1.645(16)	1.788(24)	1.791(24)	1.680(21)	1.687(22)
-O3	1.741(3)	1.691(21)	1.691(21)	1.696(24)	1.737(24)	1.803(25)	1.646(15)	1.646(15)	1.663(17)	1.651(16)
-O4	1.747(3)	1.815(14)	1.805(15)	1.799(16)	1.793(15)	1.749(17)	1.611(16)	1.614(16)	1.639(17)	1.637(17)
<Al-O>	1.733(2)	1.712(9)	1.710(9)	1.716(10)	1.727(10)	1.735(10)	1.695(10)	1.696(10)	1.673(10)	1.672(10)
Al-O1-Si	142.3(2)	151.6(6)	152.2(6)	152.7(6)	152.8(6)	152.9(6)	153.7(6)	153.4(6)	152.2(6)	151.0(6)
Al-O2-Si	152.8(2)	155.3(5)	155.5(5)	155.8(5)	156.3(5)	156.7(4)	157.8(4)	157.6(4)	158.3(4)	157.8(4)
Al-O3-Si	132.8(2)	142.7(10)	142.8(10)	142.3(11)	140.5(12)	138.4(14)	139.2(11)	139.0(10)	140.3(9)	140.1(10)
Al-O4-Si	132.9(2)	125.2(9)	126.1(9)	127.2(11)	129.9(13)	135.3(16)	134.1(11)	134.0(11)	132.5(9)	132.9(10)
<T-O-T>	140.2(1)	143.7(4)	144.2(4)	144.5(4)	144.9(5)	145.8(6)	146.2(4)	146.0(4)	145.8(4)	145.5(4)
Na2-O1	2.507(3)	2.550(9)	2.561(9)	2.577(10)	2.588(11)	2.588(10)	2.611(9)	2.610(9)	2.588(10)	2.596(10)
-O3	2.427(4)	2.583(16)	2.579(17)	2.568(18)	2.534(18)	2.490(19)	2.633(16)	2.630(16)	2.618(17)	2.617(17)
-O3	2.859(3)	2.800(15)	2.794(16)	2.788(17)	2.772(19)	2.763(21)	2.574(18)	2.566(18)	2.618(19)	2.612(19)
-O4	2.444(3)	2.293(17)	2.320(19)	2.352(22)	2.422(24)	2.503(24)	2.424(15)	2.423(15)	2.404(21)	2.395(21)
-O4	2.891(6)	2.945(15)	2.939(16)	2.928(17)	2.899(18)	2.850(19)	3.020(16)	3.031(15)	2.983(19)	3.001(19)
-OC1 ^a	2.412(12)	2.608(27)	2.638(27)	2.662(30)	2.629(31)	2.552(30)	2.540(31)	2.542(31)	2.18(5)	2.24(5)
-OC1 ^b	2.440(11)	2.17(4)	2.16(4)	2.16(4)	2.18(5)	2.26(6)	2.73(5)	2.73(5)	2.28(5)	2.24(5)
-OC1 ^b	2.431(21)	2.65(4)	2.66(4)	2.65(4)	2.65(5)	2.65(6)	2.18(5)	2.17(5)	3.01(5)	3.04(6)
<with OC1>	2.551(4)	2.575(9)	2.581(9)	2.586(9)	2.584(11)	2.582(12)	2.589(11)	2.588(11)	2.585(12)	2.593(13)
Na2-OC2 ^b	2.414(14)	2.338(26)	2.333(27)	2.345(32)	2.40(4)	2.56(4)	2.49(4)	2.49(4)	2.82(4)	2.76(5)
-OC2 ^a	2.424(21)	2.29(5)	2.26(4)	2.21(5)	2.10(4)	1.986(31)	2.929(34)	2.952(34)	2.54(6)	2.63(6)
-OC2 ^a	2.432(12)	2.66(4)	2.70(4)	2.74(4)	2.83(4)	2.954(30)	1.99(4)	1.98(4)	2.26(6)	2.19(6)
<with OC2>	2.550(4)	2.557(9)	2.561(9)	2.564(09)	2.568(11)	2.587(12)	2.584(11)	2.585(11)	2.604(12)	2.600(13)
C1-OC1 x3	1.268(9)	1.258(24)	1.255(24)	1.252(28)	1.261(31)	1.270(29)	1.290(28)	1.290(29)	1.286(34)	1.28(4)
C2-OC2 x3	1.302(9)	1.321(23)	1.333(24)	1.362(28)	1.384(31)	1.335(28)	1.417(29)	1.436(30)	1.363(32)	1.40(4)
<C-O>	1.285(4)	1.290(9)	1.294(9)	1.307(11)	1.323(13)	1.303(12)	1.354(12)	1.363(12)	1.325(14)	1.340(16)
Na1-O1 x3	2.863(3)	2.888(7)	2.881(7)	2.871(7)	2.861(7)	2.850(7)	2.852(7)	2.847(7)	2.857(7)	2.838(7)
-O2 x3	2.450(5)	2.521(6)	2.524(6)	2.531(6)	2.543(6)	2.567(5)	2.587(5)	2.586(5)	2.596(5)	2.593(5)
<Na1-O>	2.657(2)	2.705(3)	2.703(3)	2.701(3)	2.702(3)	2.709(2)	2.720(2)	2.717(2)	2.727(2)	2.716(2)
Na1-O _w ^a	2.335(23)	2.190(18)	2.184(20)	2.173(24)	2.136(31)	1.80(5)	1.63(5)	1.59(6)	1.60(12)	1.60(15)
-O _w ^b	2.874(15)	2.926(18)	2.940(20)	2.964(24)	3.016(31)					

TABLE 2.—EXTENDED

648	693	800	891	952
0.3272(8)	0.3274(8)	0.3368(11)	0.3317(14)	0.3313(16)
0.4099(8)	0.4102(8)	0.4153(8)	0.4127(8)	0.4121(10)
1.36(7)	1.49(7)	1.65(8)	1.91(8)	2.22(11)
0.0726(8)	0.0724(8)	0.0760(8)	0.0738(9)	0.0727(11)
0.4124(8)	0.4121(8)	0.4071(8)	0.4104(9)	0.4109(11)
0.7493(30)	0.7498(30)	0.7494(33)	0.752(4)	0.752(5)
0.2020(19)	0.2025(19)	0.2098(21)	0.2061(21)	0.2087(22)
0.4088(6)	0.4087(6)	0.4082(6)	0.4079(6)	0.4109(8)
0.6713(24)	0.6733(25)	0.6807(26)	0.6850(29)	0.680(4)
2.44(13)	2.46(14)	2.53(14)	2.56(14)	2.47(19)
0.1056(5)	0.1049(5)	0.1037(5)	0.1028(5)	0.1020(6)
0.5586(17)	0.5584(17)	0.5557(26)	0.5579(20)	0.5603(21)
0.7416(33)	0.7418(33)	0.7323(33)	0.7334(36)	0.747(5)
0.0092(12)	0.0080(12)	0.0043(13)	0.0013(14)	-0.0040(18)
0.3348(14)	0.3333(14)	0.3289(13)	0.3291(16)	0.3280(22)
0.0175(29)	0.0175(30)	0.0116(31)	0.0072(33)	0.003(5)
0.3171(16)	0.3172(16)	0.3201(15)	0.3169(17)	0.3177(22)
0.3584(13)	0.3585(13)	0.3595(12)	0.3560(15)	0.3561(21)
0.0662(25)	0.0655(25)	0.0613(24)	0.0558(26)	0.051(4)
0.1038(26)	0.1081(27)	0.1089(29)	0.1070(31)	0.1170(44)
7.91(20)	8.37(21)	8.93(22)	10.00(24)	10.80(33)
0.1278(15)	0.1279(15)	0.1295(15)	0.1290(15)	0.1301(19)
0.2525(5)	0.2529(5)	0.2525(5)	0.2540(6)	0.2545(8)
0.2949(17)	0.2950(18)	0.2958(21)	0.2921(24)	0.2855(32)
0.582(8)	0.576(9)	0.692(10)	0.739(13)	0.770(16)
6.7(12)	7.5(13)	7.4(13)	9.2(16)	10.9(23)
0.830(9)	0.831(9)	0.933(11)	0.957(12)	0.973(17)
0.0862(40)	0.0872(42)	0.0378(58)	0.0421(62)	0.0441(86)
0.1107(38)	0.1129(40)	0.1208(30)	0.1243(28)	0.1245(38)
0.0490(48)	0.0499(51)	0.0384(52)	0.0437(81)	0.039(11)
0.1271(26)	0.1286(28)	0.1268(36)	0.1177(33)	0.1219(49)
0.371(3)	0.371(3)	0.371(3)	0.360(3)	0.366(5)

TABLE 3.—Extended

648	693	800	891	952
1.631(24)	1.622(24)	1.609(25)	1.603(26)	1.594(28)
1.612(22)	1.606(22)	1.551(33)	1.562(28)	1.532(29)
1.644(13)	1.643(13)	1.658(15)	1.650(15)	1.630(21)
1.744(14)	1.743(14)	1.734(14)	1.717(15)	1.697(20)
1.658(9)	1.654(9)	1.638(12)	1.633(11)	1.613(12)
1.711(25)	1.719(25)	1.729(26)	1.732(27)	1.771(30)
1.684(22)	1.687(22)	1.739(34)	1.722(28)	1.744(30)
1.659(16)	1.666(16)	1.662(17)	1.652(20)	1.656(25)
1.643(16)	1.644(17)	1.643(17)	1.674(18)	1.682(23)
1.674(10)	1.679(10)	1.694(12)	1.695(12)	1.713(14)
151.8(6)	152.4(6)	155.1(7)	156.1(7)	154.5(10)
158.4(4)	158.9(4)	158.7(5)	159.5(5)	160.6(6)
140.1(9)	139.6(9)	138.6(9)	139.8(11)	141.0(16)
132.4(10)	132.7(10)	133.2(10)	133.5(11)	134.7(15)
145.7(4)	145.9(4)	146.4(4)	147.2(4)	147.7(5)
2.597(10)	2.602(11)	2.631(12)	2.655(14)	2.684(18)
2.642(17)	2.640(17)	2.681(17)	2.699(20)	2.748(29)
2.576(19)	2.562(20)	2.486(21)	2.492(24)	2.472(31)
2.395(20)	2.398(21)	2.427(16)	2.408(21)	2.403(28)
2.998(18)	2.997(19)	3.012(19)	2.964(21)	2.981(28)
2.19(5)	2.15(6)	2.54(5)	2.74(6)	2.91(8)
2.30(5)	2.32(6)	2.76(7)	2.70(8)	2.68(11)
3.00(6)	3.01(6)	2.17(7)	2.17(8)	2.18(11)
2.587(13)	2.585(14)	2.588(15)	2.604(17)	2.632(23)
2.78(4)	2.77(5)	2.36(5)	2.31(6)	2.21(8)
2.60(6)	2.60(7)	2.83(6)	2.76(10)	2.90(14)
2.21(6)	2.22(6)	2.18(6)	2.38(9)	2.35(12)
2.600(13)	2.599(14)	2.576(15)	2.584(17)	2.594(23)
1.28(4)	1.30(4)	1.36(4)	1.39(4)	1.39(5)
1.407(31)	1.424(33)	1.43(4)	1.31(4)	1.37(5)
1.344(15)	1.362(15)	1.395(16)	1.350(16)	1.380(20)
2.851(7)	2.852(7)	2.866(7)	2.876(8)	2.837(9)
2.599(5)	2.603(5)	2.604(6)	2.622(6)	2.639(8)
2.725(2)	2.728(2)	2.735(3)	2.749(3)	2.738(3)

reflections was used to determine the cell parameters, and (2) peak positions were obtained from peak-height positions rather than a least-squares fit to the whole trace (see Hassan 1996b). Note that the satellite reflections also disappear in the XRD traces at 504 °C, which is consistent with the results based on the temperature dependence of the unit-cell parameters.

The volume thermal expansivity was obtained by fitting all the cell-volume data simultaneously to the expression:

$$V(T) = V_{Tr} \exp \left[\int_{Tr}^T \alpha_V(T) dT \right]$$

where $V(T)$ is the volume at any temperature T , V_{Tr} is the volume at reference temperature, usually room temperature, and $\alpha_V(T)$ is a polynomial expression for the volume thermal expansion coefficient: $\alpha_V(T) = a_0 + a_1T + a_2T^2$. Ignoring the quadratic term, the values: $a_0 = 4.1539 (\pm 0.37) \times 10^{-5}$ and $a_1 = 1.7955 (\pm 1.63) \times 10^{-8}$ were obtained with $V_{Tr} = 702.452(2) \text{ \AA}^3$ at 25 °C for the range 25–496 °C, and $a_0 = -2.3882 (\pm 1.58) \times 10^{-5}$ and $a_1 = 9.2014 (\pm 2.23) \times 10^{-8}$ were obtained with $V_{Tr} = 716.67(3) \text{ \AA}^3$ at 511 °C for the range 511–982 °C.

For the linear thermal expansion coefficients, the a_0 and a_1 parameters were obtained by fitting the unit-cell data given in Table 1. For the a unit-cell data, $a_0 = 8.9595 (\pm 0.84) \times 10^{-6}$ and $a_1 = 7.7009 (\pm 3.7) \times 10^{-9}$ were obtained with $a_{Tr} = 12.5906(2) \text{ \AA}^3$ at 25 °C for the range 25–496 °C, and $a_0 = -0.11481 (\pm 0.38) \times 10^{-6}$ and $a_1 = 1.6582 (\pm 0.536) \times 10^{-8}$ were obtained with $a_{Tr} = 12.6508(2) \text{ \AA}^3$ at 511 °C for the range 511–982 °C. The fit to the c unit-cell data yielded, $a_0 = 2.3437 (\pm 0.20) \times 10^{-5}$ and $a_1 = 3.2326 (\pm 8.98) \times 10^{-9}$ were obtained with $c_{Tr} = 5.1168(1) \text{ \AA}^3$ at 25 °C for the range 25–496 °C, and $a_0 = -2.2912 (\pm 0.824) \times 10^{-5}$ and $a_1 = 5.7839 (\pm 1.16) \times 10^{-8}$ were obtained with $c_{Tr} = 5.1707(1) \text{ \AA}^3$ at 511 °C for the range 511–982 °C. The percent volume change from 25 to 496 °C is 2.1(2)%, from 511 to 982 °C is 2.3(4)%, and from 25 to 982 °C is 4.3(2)%.

Structure of cancrinite

The close agreement between our room-temperature structure and that of Grundy and Hassan (1982) suggested that some meaningful structural changes could be extracted from the present Rietveld structure refinements. Although there is good agreement with the mean bond distances in the tetrahedral (Al, Si) sites, the individual T-O distances are highly scattered in the powder-data refinements, whereas they are very near to the mean value in the single-crystal refinement, indicating that the present data may not be adequate to elucidate fine structural details.

At 25 °C, the average <Al-O> and <Si-O> distances are 1.712(9) and 1.621(9) Å, respectively, and they compare well with the values of 1.733(2) and 1.612(2) Å obtained by Grundy and Hassan (1982), indicating that the Al and Si atoms are fully ordered (Table 3). The relatively small variation in average <T-O> distances suggests that Al/Si ordering is maintained at temperature (Table 3; Fig. 4a). The variations of the Al-O-Si bridging angles are shown in Fig. 4b. The average <Al-O-Si> angle increases from 143.7(4) to 147.7(5)° over the temperature range of the experiments.

The Na1 site is coordinated to six O atoms of the framework and to one O_w of the H_2O molecule that is at a short distance compared to the other symmetry related H_2O molecule (Table

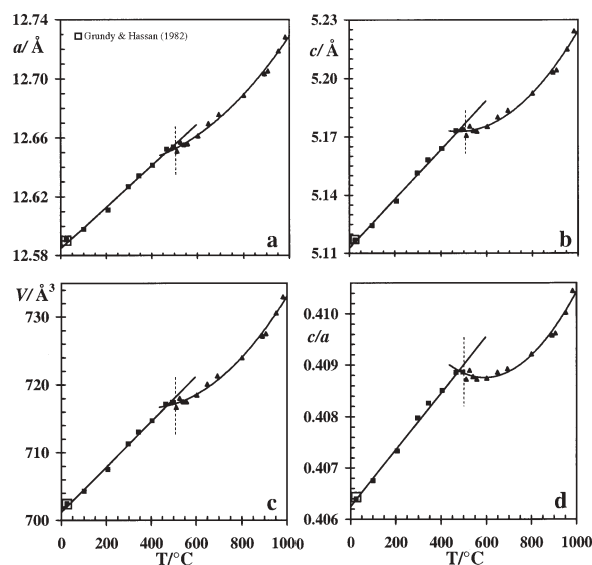


FIGURE 3. Variation of the unit-cell parameters with temperature: (a) a vs. T ; (b) c vs. T ; (c) V vs. T ; and (d) c/a vs. T . The solid and curve lines are from least-square fits to the data. Discontinuities occur in the cell parameters at 504 °C and are indicated by broken vertical lines. Data at 20 °C from Grundy and Hassan (1982) are included for comparison in this and other figures and they are indicated by “opposite” symbols to that used for the present data, i.e., if one data symbol is shown as an open square, the corresponding symbol is shown as a solid square. In all figures, error bars, if not seen, are smaller than the symbols.

3). The channels contain the Na2 site and the two independent sites for the CO₃ group that give rise to two independent C-O bonds (denoted C1-O_{C1} and C2-O_{C2}). The *sof* for the Na2 site was held invariant at 1.125 (in terms of equivalent Na scattering) throughout the temperature range. The Na2 site is coordinated to five O atoms of the framework and three O atoms of a CO₃ group (either O_{C1} or O_{C2}). The Na/Ca atom on the Na2 site, therefore, has two different coordinations depending on which CO₃-group positions are occupied. For both coordinations, the average <Na2-O> distances are nearly identical at all temperatures (Table 3; Fig. 4c). The CO₃ group was constrained to be planar (same τ for the C and O atom). Because the CO₃ group is rigid, the C-O bond distances should remain essentially constant with temperature; however they do vary slightly probably because powder rather than single-crystal diffraction data were used in this study (Table 3; Fig. 4a).

The cancrinite or ϵ -cages enclose [Na-H₂O]⁺ clusters. The *sof* for the Na1 site was held invariant at 1.0 at all temperatures. The average <Na1-O> distance increases slightly, but linearly to 952 °C (Fig. 4c). In particular, the Na1-O2 distance increases with temperature (Fig. 4c).

The O_w site is disordered around the threefold axis to form favorable hydrogen bonds and reasonable Na1-O_w distance (see Fig. 1; Grundy and Hassan 1982). In the present structure refinements, the O_w was placed on the threefold axis to help stabilize the refinements (Fechtelkord et al. 2001). As a result, the Na1-O_w distance appears short when compared to that of the disordered model (for example, at room temperature it is 2.19(2) instead

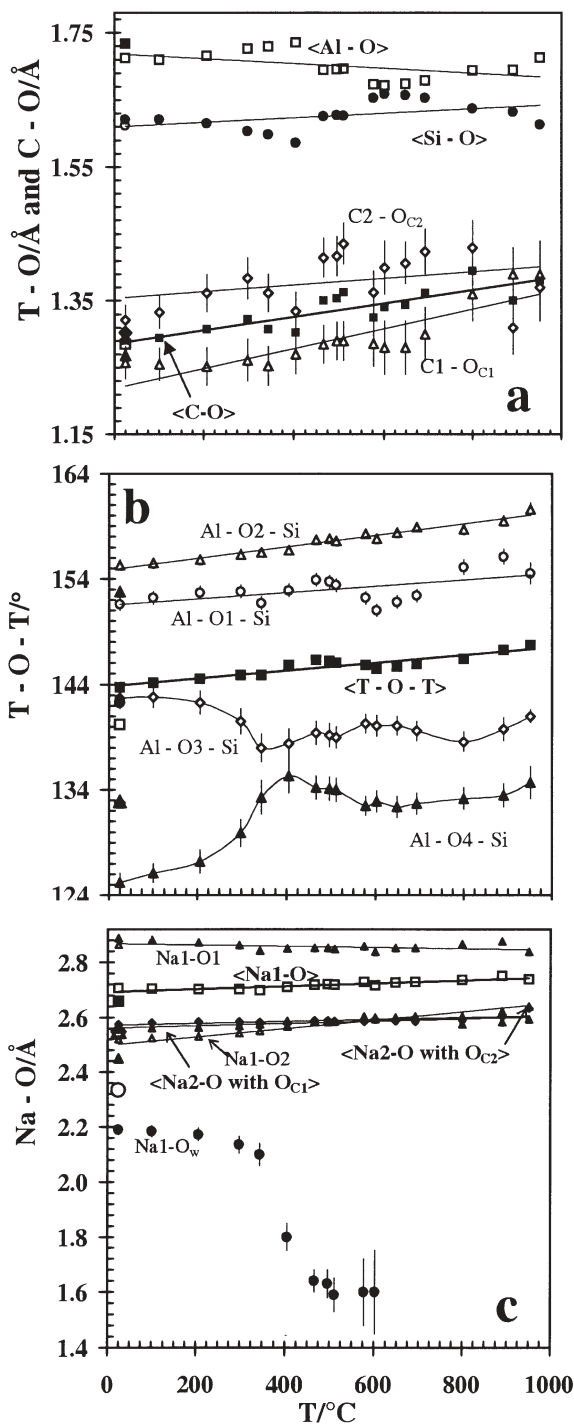


FIGURE 4. Variations of structural parameters with temperature: (a) T-O and C-O vs. T ; (b) T-O-T vs. T ; and (c) Na-O vs. T .

of 2.34(2) Å; Table 3). At higher temperatures (400 to 600 °C), the Na1-O_w distances are unrealistically short because of the real disorder of O_w and the small amount of electron density that remains in the O_w site because of the loss of water (Table 3; Fig. 4c). The single-crystal study of Grundy and Hassan (1982) showed that O_w had the largest displacement parameter, so plac-

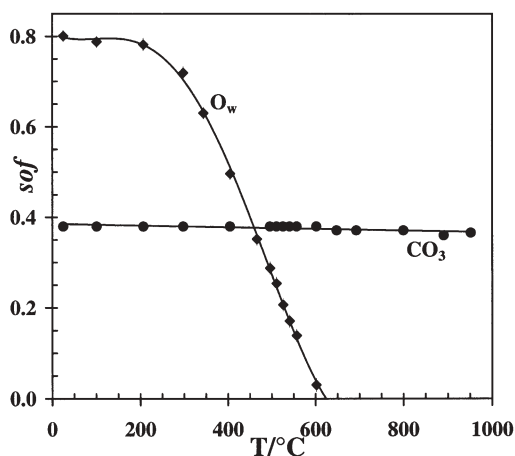


FIGURE 5. Variation of the site occupancy factors (*sofs*) for the O_w site and the atoms of the CO_3 group with temperature.

ing the O_w on the threefold axis would give rise to even larger values. Therefore, the displacement parameter for O_w was fixed at 0.025 \AA^2 throughout. Keeping O_w on the threefold axis and its displacement parameter fixed at 0.025 \AA^2 , the *sof* for O_w was refined to follow the loss of water. At room temperature, the *sof* for O_w was 0.8 instead of 1.0, the value used by Grundy and Hassan (1982). However, the chemical analysis indicates 1.75 H_2O , which gave a *sof* of 0.875, which compares favorably with the value of 0.8 obtained in this study. Despite some shortcomings in the structural model, the quality of the refinements was sufficient to follow the loss of water from the *sof* of O_w (Fig. 5). Based on this approach, it was found that all the water is lost at about $625 \text{ }^\circ\text{C}$ (Fig. 5). In contrast, the DTA-TG study on cancrinite shows that water is lost continuously on heating up to about $683 \text{ }^\circ\text{C}$ (Hassan 1996a). Therefore, from about 625 to $950 \text{ }^\circ\text{C}$, an anhydrous cancrinite phase must exist. An anhydrous phase has also been identified in a sample obtained by heating cancrinite to $600 \text{ }^\circ\text{C}$, and then cooling it to room temperature (Ballirano et al. 1995). The transition from the hydrous to the anhydrous cancrinite phase is quite gradual and not well-defined in the DTA study, but was observed at $683 \text{ }^\circ\text{C}$ (see peak-2 in Hassan 1996a). In this study, however, the hydrous to anhydrous transition is clearly observed at about $625 \text{ }^\circ\text{C}$.

Dehydration and thermal behavior of cancrinite

In cancrinite, all the H_2O is lost by about $625 \text{ }^\circ\text{C}$; an anhydrous cancrinite phase exists from about 625 to $952 \text{ }^\circ\text{C}$ (Fig. 5). The structure refinement at $952 \text{ }^\circ\text{C}$ shows negligible loss of CO_2 (Table 3; Fig. 5).

The thermal-expansion curves for cancrinite show a break at $504 \text{ }^\circ\text{C}$, where the superstructure is destroyed and a phase transition occurs. The chemical formula used in the refinements is $Na_6Ca_{1.52}[Al_6Si_6O_{24}](CO_3)_{1.52} \cdot 2H_2O$, which indicates 0.48 $[Ca-CO_3]$ vacancies in the channels. These vacancies are ordered and give rise to the supercell in cancrinite. On heating, the ordering of the $[Ca-CO_3]$ clusters and vacancies in the channels is destroyed at $504 \text{ }^\circ\text{C}$. During the disordering process, the structure adjusts slightly as indicated by the small changes in

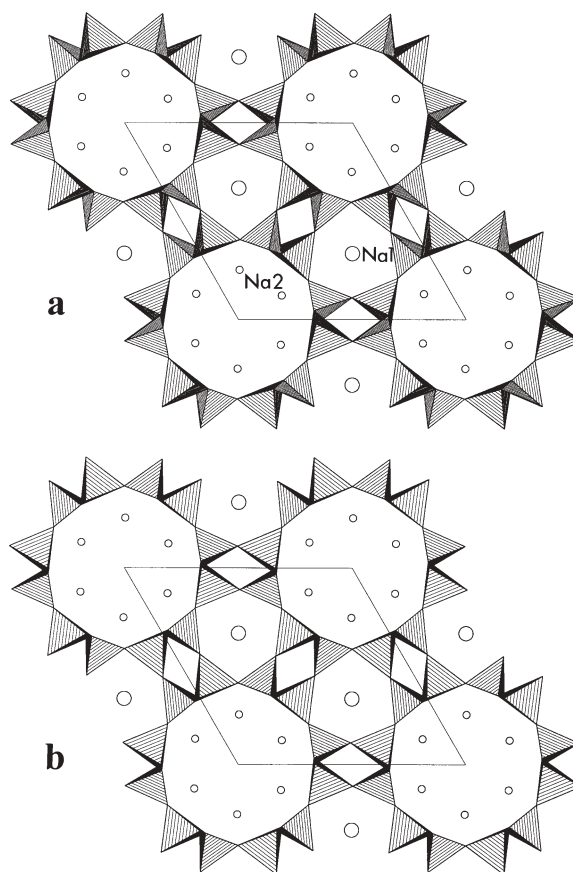


FIGURE 6. Comparison of the cancrinite framework structure: (a) at $25 \text{ }^\circ\text{C}$; and (b) at $952 \text{ }^\circ\text{C}$. At high temperatures, the tetrahedra rotate in a cooperative manner with respect to those at low temperatures. The rotation is best seen by comparing an identical tetrahedron at both temperatures.

bond distances and angles (Fig. 4).

In sodalite, the angle of rotation of the framework tetrahedra is comparable to the change in the Al-O-Si angle. In cancrinite, from 25 to $952 \text{ }^\circ\text{C}$, the average $\langle Al-O-Si \rangle$ angle increases by $4.0(6)^\circ$ compared to that of $7.8(2)^\circ$ in sodalite for a comparable temperature range (Hassan et al. 2004). The rotation of the framework tetrahedra in cancrinite is illustrated in Figure 6, where the structures at 25 and $952 \text{ }^\circ\text{C}$ are compared. The cooperative rotation of the tetrahedra, which is caused by the increase in Na1-O2 distances with temperature (Fig. 4c), gives rise to the expansion in cancrinite.

ACKNOWLEDGMENTS

We thank the anonymous reviewers for useful comments. This research was carried out in part at the National Synchrotron Light Source, Brookhaven National Laboratory (BNL), which is supported by the U.S. Department of Energy, Division of Materials Sciences and Division of Chemical Sciences, under contract no. DE-AC02-98CH10886. Jonathan C. Hanson of Brookhaven National Laboratory is thanked for his help in performing the synchrotron experiments. This study was financially supported by NSF grants EAR-0125094 and EAR-0510501.

REFERENCES CITED

- Ballirano, P. and Maras, A. (2004) The crystal structure of a "disordered" cancrinite. *European Journal of Mineralogy*, 16, 135–141.
- Ballirano, P., Maras, A., Caminiti, R., and Sadun, C. (1995) Carbonate-cancrinite:

- in-situ real-time processes studied by means of energy-dispersive X-ray powder-diffraction. *Powder Diffraction*, 10, 173–177.
- Bonaccorsi, E., Merlino, S., and Pasero, M. (1990) Davyne: its structural relationships with cancrinite and vishnevite. *Neues Jahrbuch für Mineralogie-Monatshefte*, 3, 97–112.
- Bonaccorsi, E., Merlino, S., Orlandi, P., Pasero, M., and Vezzalini, G. (1994) Quadridavynite, $[(\text{Na,K})_6\text{Cl}_2][\text{Ca}_2\text{Cl}_2[\text{Si}_6\text{Al}_6\text{O}_{24}]]$, a new feldspathoid mineral from Vesuvius area. *European Journal of Mineralogy*, 6, 481–487.
- Bonaccorsi, E., Merlino, S., Pasero, M., and Macedonio, G. (2001) Microsommitite: crystal chemistry, phase transitions, Ising model and Monte Carlo simulations. *Physics and Chemistry of Minerals*, 28, 509–522.
- Brown, W.L. and Cesbron, F. (1973) Sur les surstructures des cancrinites. *Comptes Rendus Hebdomadaires des Seances de L'Academie des Sciences Paris*, 276, Série D, 1–4.
- Burton, A., Feuerstein, M., Lobo, R.F., and Chan, J.C.C. (1999) Characterization of cancrinite synthesized in 1,3-butanediol by Rietveld analysis of powder neutron diffraction data and solid-state ^{23}Na NMR spectroscopy. *Microporous and Mesoporous Materials*, 30, 293–305.
- Emiraliyev, A. and Yamzin, I.I. (1982) Neutron-diffraction refinement of the structure of carbonate-cancrinite. *Soviet Physics Crystallography*, 27, 27–30.
- Fechtelkord, M., Stief, F., and Buhl, J.-C. (2001) Sodium cation dynamics in a nitrate cancrinite: A low and high temperature ^{23}Na and ^1H MAS NMR study and high temperature Rietveld structure refinement. *American Mineralogist*, 86, 165–175.
- Foit, F.F., Jr., Peacor, D.R., and Heinrich, E.W.M. (1973) Cancrinite with a new superstructure from Bancroft, Ontario. *Canadian Mineralogist*, 11, 940–951.
- Grundy, H.D. and Hassan, I. (1982) The crystal structure of a carbonate-rich cancrinite. *Canadian Mineralogist*, 20, 239–251.
- Hammersley, J. (1996) Fit2d user manual. ESRF publication, Grenoble, France.
- Hassan, I. (1996a) The thermal behavior of cancrinite. *Canadian Mineralogist*, 34, 893–900.
- — — (1996b) Thermal expansion of cancrinite. *Mineralogical Magazine*, 60, 949–956.
- Hassan, I. and Buseck, P.R. (1992) The origin of the superstructure and modulations in cancrinite. *Canadian Mineralogist*, 30, 49–59.
- Hassan, I. and Grundy, H.D. (1984) The character of the cancrinite-vishnevite solid-solution series. *Canadian Mineralogist*, 22, 333–340.
- — — (1990) Structure of davynite and implications for stacking faults. *Canadian Mineralogist*, 28, 341–349.
- — — (1991) The crystal structure of basic cancrinite, ideally $\text{Na}_8[\text{Al}_6\text{Si}_6\text{O}_{24}](\text{OH})_2 \cdot 3\text{H}_2\text{O}$. *Canadian Mineralogist*, 29, 377–383.
- Hassan, I., Antao, S.M., and Parise, J.B. (2004) Sodalite: high-temperature structures obtained from synchrotron radiation and Rietveld refinements. *American Mineralogist*, 89, 359–364.
- Jarchow, O. (1965) Atomanordnung und Strukturverfeinerung von Cancrinit. *Zeitschrift für Kristallographie Kristallphysik Kristallchemie*, 122, 407–422.
- Kanepit, V.N. and Nozik, Y.Z. (1985) A neutron-diffraction study of cancrinite. *Geokhimiya*, 7, 1058–1062.
- Larson, A.C. and Von Dreele, R.B. (2000) General Structure Analysis System (GSAS). Los Alamos National Laboratory Report, LAUR 86-748.
- Merlino, S., Mellini, M., Bonaccorsi, E., Pasero, M., Leoni, L., and Orlandi, P. (1991) Pitiglianoite, a new feldspathoid from southern Tuscany, Italy: chemical composition and crystal structure. *American Mineralogist*, 76, 2003–2008.
- Nithollon, P. and Vernotte, M.P. (1955) Structure cristalline de la cancrinite. *Publications scientifiques et techniques du ministère de l'air (France)*, Notes Techniques 53, 1–48.
- Peacor, D.R., Rouse, R.C., and Ahn, J.-H. (1987) Crystal structure of tiptopite, a framework beryllophosphate isotopic with basic cancrinite. *American Mineralogist*, 72, 816–820.
- Smolin, Y.I., Shepelev, Y.F., Butikova, I.K., and Kobayakov, I.B. (1981) Crystal structure of cancrinite. *Soviet Physics Crystallography* 26, 33–35.
- Toby, B.R. (2001) EXPGUI, a graphical user interface for GSAS. *Journal of Applied Crystallography*, 34, 210–221.
- Weller, M.T. and Kenyon, N.J. (2004) Investigation of cancrinite structures by powder neutron diffraction. *Recent Advances in the Science and Technology of Zeolites and Related Materials*, parts A–C, *Studies in Surface Science and Catalysis*, 154, 1349–1355.

MANUSCRIPT RECEIVED JUNE 20, 2005

MANUSCRIPT ACCEPTED FEBRUARY 6, 2006

MANUSCRIPT HANDLED BY SIMONA QUARTIERI